Sharp/tuneable UVC selectivity and extreme solar blindness in nominally undoped Ga2O3 MSM photodetectors grown by pulsed laser deposition

D. J. Rogers, A. Courtois, F. H. Teherani, V. E. Sandana, P. Bove, Xavier Arrateig, Luc Damé, P. Maso, Mustapha Meftah, W. El Huni, et al.

Sharp/Tuneable UVC Selectivity and Extreme Solar Blindness in Nominally Undoped Ga$_2$O$_3$ MSM Photodetectors Grown by Pulsed Laser Deposition

D. J. Rogers[1*], A. Courtois[1], F. H. Teherani[1], V. E. Sandana[1], P. Bove[1], X. Arrateig[2], L. Damé[2], P. Maso[3], M. Meftah[2], W. El Huni[4], Y. Sama[4], H. Bouhnane[4], S. Gautier[4], A. Ougazzaden[5] & M. Razeghi[6]

[1] Nanovation, 8 route de Chevreuse, 78117 Châteaufort, France

[2] LATMOS, CNRS, Université de Versailles Saint-Quentin-en-Yvelines, Université Paris-Saclay, Sorbonne Université (SU), 11 Boulevard d'Alembert, 78280 Guyancourt, France

[3] Université Paris-Saclay, UVSQ, CNRS, OVSQ-PIT, 78280, Guyancourt, France.

[4] Institut Lafayette, 2 rue Marconi, 57070 Metz, France

[5] Georgia Institute of Technology, School of Electrical & Computer Engineering, GT-Lorraine, 57070 Metz, France

[6] Center for Quantum Devices, ECE Department, Northwestern University, Evanston, Illinois, USA

*E-mail: rogers@nanovation.com

ABSTRACT

Ga$_2$O$_3$ layers were grown on c-sapphire substrates by pulsed laser deposition. Optical transmission spectra were coherent with a bandgap engineering from 4.9 to 6.2 eV controlled via the growth conditions. X-ray diffraction revealed that the films were mainly β-Ga$_2$O$_3$ (monoclinic) with strong (-201) orientation. Metal-Semiconductor-Metal photodetectors based on gold/nickel Inter-Digitated-Transducer structures were fabricated by single-step negative photolithography. 240 nm peak response sensors gave over 2 orders-of-magnitude of separation between dark and light signal with state-of-the-art solar and visible rejection ratios (($I_{240} : I_{290}$) of $> 3 \times 10^5$ and ($I_{240} : I_{400}$) of $> 2 \times 10^6$) and dark signals of <50 pA (at a bias of -5V). Spectral responsivities showed an exceptionally narrow linewidth (16.5 nm) and peak values exhibited a slightly superlinear increase with applied bias up to a value of 6.5 A/W (i.e. a quantum efficiency of $> 3000\%$) at 20V bias.

1. INTRODUCTION

Ultraviolet (UV) photodetectors (PD) are emerging for applications such as flame/spark detection, chemical/biological-agent detection, military counter-measures, environmental monitoring, UV sterilization monitoring, non-line-of-sight communications and UV space astronomy [1-4]. To minimize false alarms and background clutter, many of these devices operate in the solar-blind (SB) UVC portion of the spectrum (<290 nm). Most current PD employ photomultipliers (PMs). These are based on vacuum tubes, which are bulky, fragile (mechanically and electrically) expensive and require high operating voltages. Solid-state SBPDs, based on quantum transitions in semiconductors, are much more robust than PMs and promise both size and cost advantages compared to PMs. They also have the potential for higher quantum efficiency, intrinsic spectral range selectivity, extended lifetimes, lower noise

and lower power requirements. Silicon photodiodes have long been used for UV detection. Although they work well, their bandgap is relatively low, so they respond to the visible spectrum as well UV signals and require optical filters in order to be either visible or solar blind. A class of materials called "wide bandgap (WBG)" semiconductors, are naturally visible blind, however. Figure 1 contrasts the wavelength operating range that can be attained for common WBG optosemiconductors. Silicon carbide (SiC), with a room-temperature bandgap of 2.4–3.1 eV, was the first WBG semiconductor to be adopted commercially as a UVC PD (eg in flame detectors) [5]. However, the bandgap of SiC is not high enough for it to be intrinsically SB, and bandgap engineering through alloying is not possible. Thus, insertion of optical filters is still necessary in order to tune the photodetection to the UVC range. Gallium nitride (GaN), on the other hand, has a bandgap which is tunable from the near to far UV range through alloying with aluminium, and (Al)GaN based devices have been widely explored for detection of UV light right into the SB range [6-8]. However, this material system suffers from several key problems: large dislocation densities, low conductivity and lattice/thermal expansion mismatches (with the conventional sapphire substrate) which lead to cracking and efficiency fall-off with increasing Al content. The result is that there has been limited success in demonstrating (Al)GaN based SBPDs with both low background signals and good quantum efficiencies for wavelengths under 250nm [9,10]. (Mg)ZnO is based on wurtzite ZnO, which has a direct wide bandgap of ~3.4 eV that can be tuned into the SB range by alloying with MgO (Eg ~7.8eV) [11]. The Mg ion has a similar radius to that of Zn [12], so there are less strain and efficiency drop-off concerns than for (Al)GaN. As the Mg content increases, however, the hcp ZnO phase transforms into the fcc MgO phase which is much more insulating in nature and less suitable for device applications. Thus SB operation is limited to a range over about 250nm. Although Boron Nitride (BN) and Diamond (D) have intrinsic "ultra-wide bandgaps" (UWBG) (of 6.1 and 5.5 eV, respectively) which are very attractive for SB operation [13,14] they are difficult to grow in wide area thin film form with high crystal quality and low defect densities. As for SiC, they also both have limited scope for bandgap engineering further into the UV. Hence there is a need for a more suitable semiconductor system for wavelength-selective sensing in the 200-250nm UVC range.
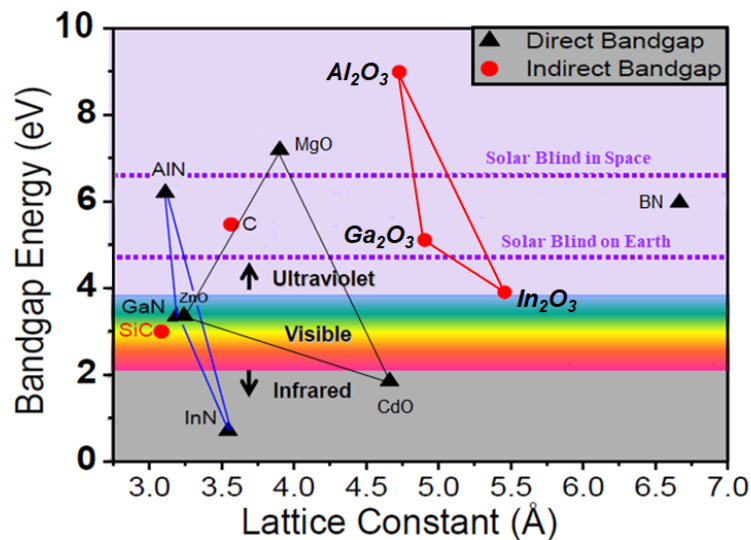

Figure 1. Bandgap engineering possibilities with the most common wide bandgap optosemiconductors.

Over the past few years, attention has turned to the UWBG (~4.9 eV) semiconductor beta gallium oxide ($\beta-Ga_2O_3$) [15,16].   This is because of recent demonstration of bandgap engineering further into the UV range by alloying with α-Al_2O_3 (Eg ~9.0eV) [17] along with the emergence of large format single crystal native substrates [18], high quality homoepitaxy [19] and n-type doping [20].

Recently, the authors demonstrated that excellent β-Ga_2O_3 Metal-Semiconductor-Metal (MSM) PDs could be made using heteroepitaxial thin films grown on non-native c-sapphire substrates by Pulsed Laser Deposition (PLD) [21].   Interestingly, it was found that the spectral responsivity peak position could be decreased by reducing film thickness. This phenomenon was attributed to Al diffusing into the layer from the Al_2O_3 substrate [17].

The studies also revealed, however, a relatively wide spectral responsivity, persistent photoconductivity and a significant detection tail extending into the UVB and UVA, which were all attributed to defects in the material [22].

The aim of this study was to explore the possibilities of further engineering the bandgap into the UV and reducing the defect-related limitations on the device performance.

2. EXPERIMENT

Nominally undoped Ga_2O_3 epilayers were grown on c-plane sapphire (c-Al_2O_3) substrates in a Surface GmbH PLD system using a commercial sintered target and a Coherent LPX KrF (λ = 248nm) laser, as described elsewhere [23].   Uniform 2-inch-diameter-wafer coverage was obtained using optical rastering of the incident laser beam over the target surface.   The system was equipped with a Riber radio-frequency (rf) plasma source in order to supply atomic oxygen to the substrate during the film growth (see Figure 2).
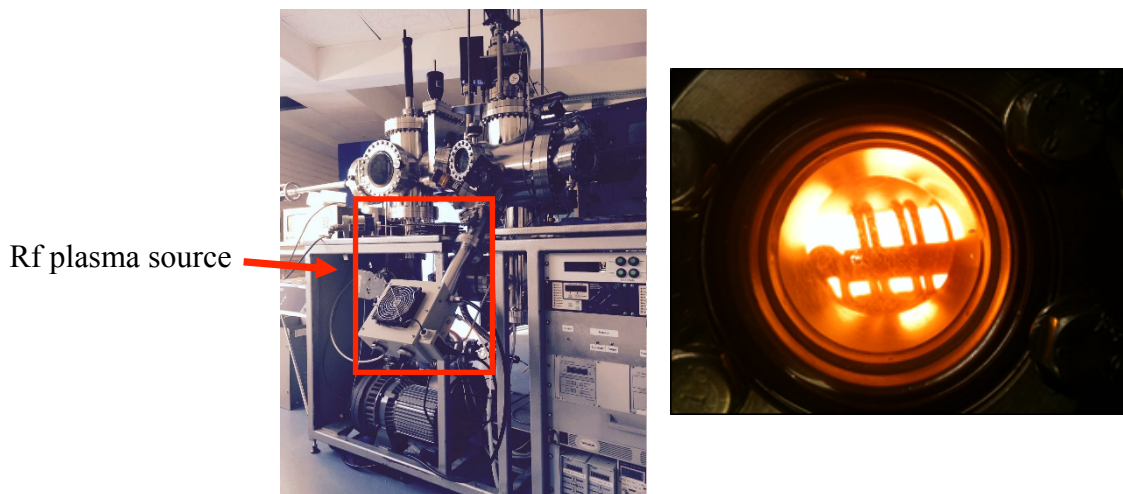

Figure 2 The Surface GmbH plasma-assisted PLD system at Nanovation, with an inset image of the rf oxygen plasma.

Room temperature (RT) optical transmission studies were performed post-growth using an Ocean Optics system comprising a halogen lamp, a deuterium lamp and a Maya optical spectrometer. The crystal structure of the samples was investigated using high resolution X-Ray Diffraction (XRD) performed in a Rigaku Smartlab system using Cu Kα_1 radiation. Electrical resistivity was measured with a Signatone four-collinear-probe system equipped with a Keithley 2400 source-meter. Hall measurements were made at room temperature in Van der Pauw configuration using an Ecopia HMS3000 system (with a 1T magnet and indium-soldered Ohmic contacts).

MSM PD were fabricated by negative photolithography using Au/Ni Interdigitated Transducer (IDT) structures. The devices had 500 fingers (2 μm x 1000 μm) with a finger spacing of 2 μm. Wafer inspection was done using a Nanotronics NSPEC system.

I/V characteristics (with/without back illumination) and spectral responsivity curves were acquired using a Karl Suss probe station equipped with a Keithley 6430 source meter, a Dynasil digital monochromator and an Ocean Optics HPX-2000-HP-DUV 75W Xe fibre optic light source (calibrated with an Ophir Nova laser power monitor).

3. RESULTS & DISCUSSION

3.1 Thin Film Characterisation

The Ga_2O_3 layers showed good transparency to the visible spectrum and +/- 5% within-wafer homogeneity of the thickness, the SB transmission spectrum and the electrical resistivity. Figure 3 shows optical transmission spectra for Ga_2O_3 layers engineered so as to have different UVC cutoffs (as described previously [20]).

Tauc plots revealed that, the corresponding bandgaps ranged from 4.9 to 6.2 eV. Hence Ga_2O_3 materials can be engineered in this way to cover the whole UVC spectral range from ~255 nm to ~ 200 nm. 200nm is, in fact, the lower limit for terrestrial UV detection since oxygen in the air absorbs light with wavelengths below this value.
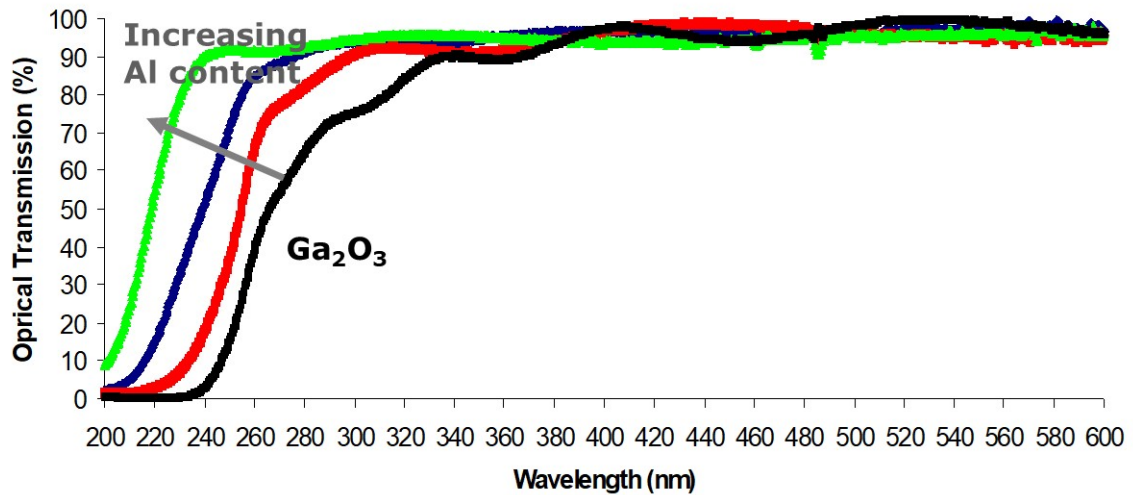
Figure 3 Optical transmission spectra for Ga_2O_3 layers as a function of Al content.

Four point resistivity and Hall measurements were not possible because the films were too resistive for the measurement electronics.

Figure 4 shows a $2\theta/\Omega$ XRD scan for the Ga_2O_3 layer for the red optical transmission spectrum shown in Figure 3.
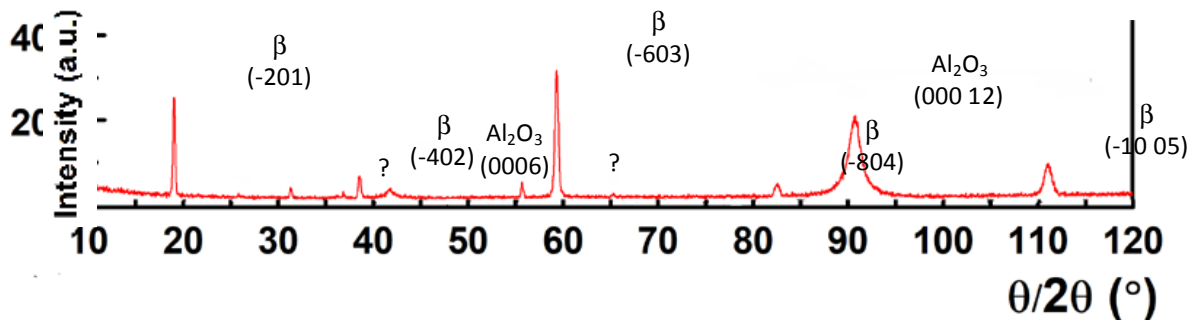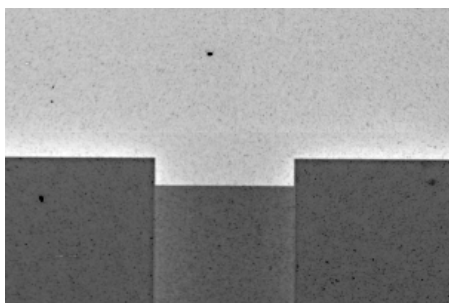

Figure 4 A typical $2\theta/\Omega$ XRD scan for a Ga_2O_3 layer grown on a c-sapphire substrate.

It can be seen from the scan that the layer has relatively narrow peaks characteristic of monoclinic β-Ga_2O_3 with a strong preferential (-201) orientation and a comparatively large grain size. There are also peaks at about 31.5° and 56° which may be attributed the (002) reflection of β-Ga_2O_3 and the (116) reflection of α-Ga_2O_3, respectively, although these attributions are not definitive. It can be concluded, however, that the layer was constituted mainly of β-Ga_2O_3.

3.2 Device Characterisation

Figure 5 shows wafer inspection and optical microscope images of the MSM IDT device after photolithography and metallization.
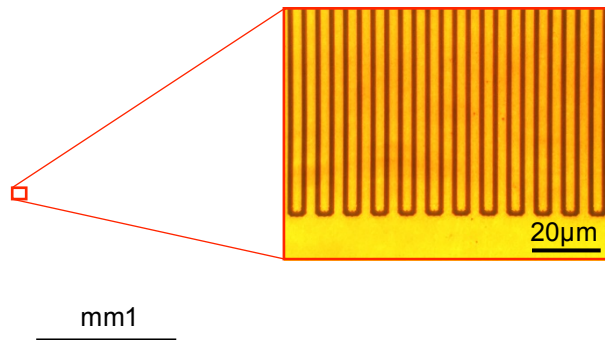
Figure 5 wafer inspection and optical microscope images of the IDT device after photolithography and metallization.

Figure 6 shows I/V curves (both with and without back illumination) for an MSM PD made from the Ga_2O_3 layer of Figure 4.
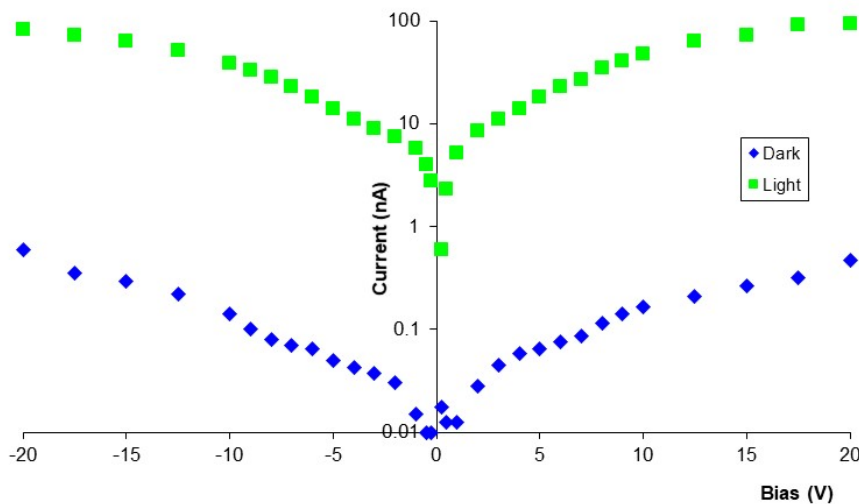

Figure 6 I/V Curves for a β-Ga_2O_3 MSM PD both with and without back illumination (2 micron finger spacing) – N.B. current is in log scale.

The I/V curves show that there was more than two orders of magnitude of separation between dark and light current. The dark current was 60pA for a bias voltage of -5V. There is a slight offset towards positive voltages for the light signal which leaves a photocurrent of a few hundreds of pA for 0V of applied bias. The same phenomenon was observed for many devices, but the origin is unclear. Some possible explanations are a photovoltaic effect, an instrumental offset (related to the very low level measurements) or a photothermal effect. The mainly Ohmic nature of the contacts makes the photovoltaic interpretation seem unlikely, however.
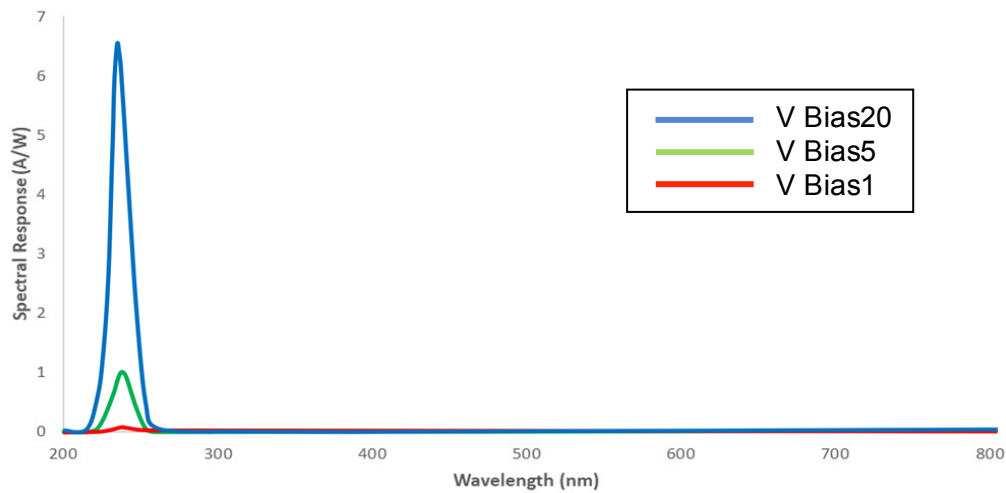Figure 7 shows a plot of spectral responsivity as a function of bias.

Figure 7 Spectral responsivity as a function of bias voltage.

The peak of the spectral responsivity is centered at approximately 240 nm for all bias voltages. This value correlates closely with the bandgap found in the optical transmission studies (see Figure 3, above) and corresponds to an Al content between about 20 and 25 at % [24]. The linewidth (a metric for spectral selectivity) was about 16.5 nm for all bias voltages. The peak responsivity value shows a slightly superlinear increase with bias voltage (up to a value of 6.5 A/W at 20V bias). This corresponds to a quantum efficiency of over 3000%. This high value of quantum efficiency is common for such detector architectures and is usually attributed to photoconductive gain due to hole trapping at the interface between the Ga_2O_3 and the metal electrode [25].

Figure 8 shows the spectral responsivity in log scale (for a bias voltage of 5V).
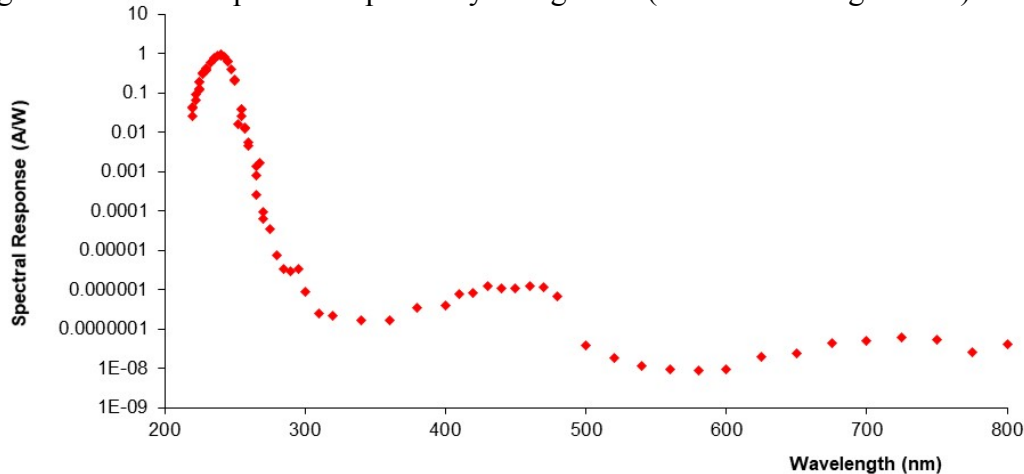

Figure 8 Spectral responsivity (in log scale) for a 5V applied bias.

The log scale plot reveals that the devices had a remarkably high solar rejection ratios ((I_{240} : I_{290}) of >3 x 10^5 and (I_{240} : I_{400}) of >2 x 10^6).

Figure 9 shows photocurrent vs time for four cycles of manual illumination shuttering (at 1V bias).
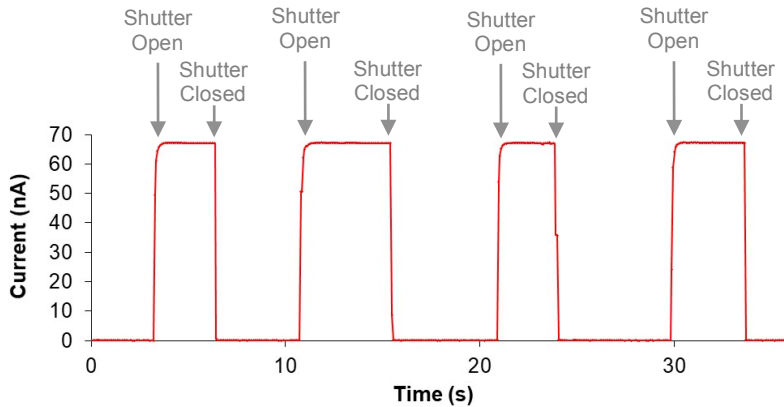

Figure 9 Photocurrent vs time for four cycles of manual illumination shuttering (at 1V bias).

The device shows sharp rise and fall times (in the ms range) upon shuttering and a slightly rounded shoulder (over less than half a second) at the top of the rise phase before repeatedly attaining a reproducible/constant photocurrent level of about 67 nA. At this scale there is no evidence of persistent photoconductivity in either the light or the dark signal.   Figure 10 shows a zoom of the dark signal during the illumination shuttering shown in Figure 9.
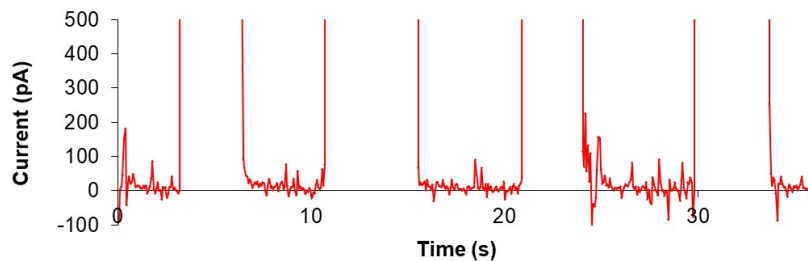

Figure 10 A zoom of the dark signal during the illumination shuttering shown in Figure 9.

At this scale of graph, it can be seen that the dark current level is in the single pA range, with a root mean square (rms) noise level of about 10pA. Upon shutter closing, the dark signal drops to under 50pA within milliseconds and then decays to the single pA range after about 3 seconds. Figure 11 shows a zoom of the peak photocurrent during the illumination shuttering shown in Figure 10.
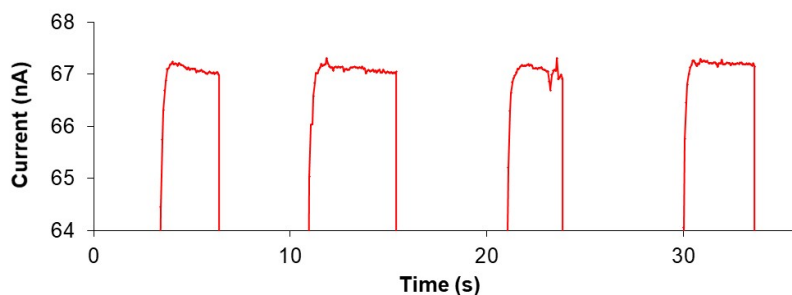
Figure 11 A zoom of the peak photocurrent during the illumination shuttering shown in Figure 10.

The figure reveals that the photocurrent signal repeatably plateaus to 67 + 0.2 nA and that there is an initial overshoot (of about 0.2nA) followed by a gradual decay and stabilization at about 67 nA.

4. CONCLUSIONS

Ga_2O_3 layers were grown on 2 inch diameter c-Al_2O_3 substrates by PLD. XRD indicated that the films were composed of mainly the monoclinic β polytype with strong preferential (-201) orientation. The bandgap was engineered from 4.9 up to 6.2 eV through control of the growth conditions. It was suggested that this was due to alloying with Al diffusing into the layer from the substrate.

MSM PDs with Au/Ni IDT were fabricated by single-step negative photolithography. IV characteristics (for 240nm peak response devices) revealed over 2 orders of magnitude of separation between dark and light signals. Spectral responsivities showed a slightly superlinear increase with applied bias and a peak responsivity of 6.5 A/W (i.e. a quantum efficiency of >3000%) was recorded at 20V bias. The main spectral response peak remained centered at 240 nm with no significant wavelength shift for biases up to 20V. Compared to previous generations of Ga_2O_3 based MSMs [21], the devices showed considerably higher solar rejection ratios ((I_{240} : I_{290}) of >3 x 10^5 and (I_{240} : I_{400}) of >2 x 10^6) and much sharper spectral selectivity (linewidth of 16.5 nm) which would make them better adapted for wavelength selective sensing and/or imaging applications. The dark signal was <50 pA (at a bias of -5V) and the rms noise level was about 10pA. Time response studies (at 1V bias) revealed sharp rises and falls (millisecond range) and no evidence of significant persistent photoconductivity.

ACKNOWLEDGEMENTS

REFERENCES

[1] J. Son Proc. of SPIE 10727 (2018) 107270F-1

[2] M. Meftah, L. Damé, P. Keckhut, S. Bekki, A. Sarkissian, A. Hauchecorne, E. Bertran, J-P Carta, D. Rogers, S. Abbaki, C. Dufour, P. Gilbert, L. Lapauw, A-J Vieau, X. Arrateig, N. Muscat, P. Bove, É. Sandana, F. Teherani, T. Li, G. Pradel, M. Mahé, C. Mercier, A. Paskeviciute, K. Segura, A. B. Alba, A. Aboulila, L. Chang , A. Chandran, P-R. Dahoo and A. Bui Remote Sens. 12, (2020) 92

[3] M. Meftah, M. Snow, L. Damé, D. Bolseé, N. Pereira, G. Cessateur, S. Bekki, P. Keckhut, A. Sarkissian and A. Hauchecorne A&A 645, A2 (2021)

[4] M. Meftah, M. Dominique, A. Ben Moussa, I.E. Dammasch, D. Bolsée, N. Pereira, L. Damé, S. Bekki and A. Hauchecorne Proc. of SPIE 10196 (2017) 1019606

[5] E. Monroy, F. Omnes; F. Calle Semicond. Sci. Technol. 18 (2003) 33

[6] R. McClintock, A. Yasan, K. Mayes, D. Shiell, S. R. Darvish, P. Kung, and M. Razeghi Appl. Phys. Lett. 84, 1248 (2004).

[7] M. Razeghi & R. McClintock in Optoelectronic Devices III-Nitride, Razeghi & Henini (2004)

[8] R. McClintock, K. Mayes, A. Yasan, D. Shiell, P. Kung and M. Razeghi Appl. Phys. Letts. 86, 011117 (2005).

[9] E. Cicek, Z. Vashaei, E.K. Huang, R. McClintock and M. Razeghi OSA Optics Letts. 37, 5, 896 (2012)

[10] E. Cicek, M. Razeghi et al. Crack-free AlGaN for SB FPA through reduced area epitaxy Appl. Phys. Letts. 102, 5 (2013) 051102-1

[11] D. J. Rogers, P. Bove, E. V. Sandana, M. Razeghi and F. Hosseini Teherani Laser Focus World feature article, 49, 10 October (2013)

[12] A. Ohtomo, M. Kawasaki, T. Koida, K. Masubichi, H. Koinuma, Y. Sakurai, Y. Yoshida, T. Yasuda & Y. Segawa Appl. Phys. Lett. 72, 19 (1998) 2466

[13] Xin Li, M. B. Jordan, T. Ayari, S. Sundaram, Y. El Gmili, S. Alam, M. Alam, G. Patriarche, P. L. Voss, J. P. Salvestrini & A. Ougazzaden Scientific Reports 7 (2017) 786

[14] M. Liao, Functional Diamond, 1, 1 (2021) 29

[15] X. Chen, F. Ren, S. Gu and J. Ye Photonics Research 7, 4 (2019)

[16] A. Pérez-Tomás, E. Chikoidze, M. R. Jennings, S. A. O. Russell, F. H. Teherani, P. Bove, E. V. Sandana and D. J. Rogers Proc. of SPIE 10533 (2018) 105331Q-1

[17] Y. Kokubun, K. Miura, F. Endo, and S. Nakagomi, Appl. Phys. Lett. 90(3), 031912 (2007).

[18] E. G. Villora, K. Shimamura, Y. Yoshiokawa, K. Aoki, N. Chinose J. Cryst. Growth 270, 3-4 (2004) 420

[19] M. Razeghi, J.-H. Park, R. McClintock, D. Pavlidis, F. H. Teherani, D. J. Rogers, B. A. Magill, G. A. Khodaparast, Y. Xu, J. Wu and V. P. Dravid Proc. of SPIE 10533 (2018) 105330R-1

[20] A. Perez-Tomas, E. Chikoidze, Y. Dumont, M. R. Jennings, Y. Kurtuluş, G. Catalana, M. Lira-Cantu, C. Ton – That, F. H. Teherani, V. E. Sandana, P. Bove and D. J. Rogers Materials Today Energy, 14 (2019) 100350

[21] D. J. Rogers, F. H. Teherani, V. E. Sandana, X. Arrateig, P. Bove, M. Razeghi, R. McClintock, E. Frisch and S. Harel Proc. of SPIE 10533 (2018) 105331P-1

[22] Y. Hou, Z. Mei & X. Du J. Phys. D : Appl. Phys. 47 (2014) 283001

[23] F. H. Teherani, D. J. Rogers, V. E. Sandana, P. Bove, C. Ton-That, L. L. C. Lem, E. Chikoidze, M. Neumann-Spallart, Y. Dumont, T. Huynh, M. R. Phillips, P. Chapon, R. McClintock & M. Razeghi Proc. of SPIE 10105 (2017) 101051R-1

[24] T. Wang, W. Li, C. Ni,_ and A. Janotti Physical Review Applied 10, 1 (2018)

[25] Y. Qin, S. Long, H. Dong, Q. He, G. Jian, Y. Zhang, X. Hou, P. Tan, Z. Zhang, H. Lv, Q. Liu and M. Liu Chinese Phys. B 28 (2019) 018501